



A SLUG-CHURN FLOW MODEL FOR SMALL-DIAMETER AIRLIFT PUMPS

F. DE CACHARD† and J. M. DELHAYE

Commissariat à l'Énergie Atomique, Centre d'Études Nucléaires de Grenoble, Service de Thermohydraulique pour les Applications Industrielles, 38054 Grenoble, Cedex 9, France

(Received 30 January 1995; in revised form 30 January 1996)

Abstract—In an airlift pumping process, air is injected into the pipe containing the fluid to be transferred. Small-diameter airlift pumps are, in particular, used for corrosive or radioactive liquids. Detailed experiments including differential pressure and void fraction measurements, are carried out on a 10 mm-diameter setup. Based on the results obtained, it is shown that existing models are not appropriate for small diameter airlifts, particularly because they overpredict the frictional pressure drop in slug flow. A new steady state airlift model is proposed. The pressure gradient in the riser is predicted by a combination of specific models describing slug and churn flow. These models are based on the available literature on two-phase flow. The particular structure of slug flow is accounted for by a cellular model. The model proposed represents an accurate analysis tool for the design of small diameter (up to 40 mm), tall (length-to-diameter ratio greater than 250) airlifts. Copyright © 1996 Elsevier Science Ltd.

Key Words: airlift pumps, two-phase flow, slug flow, churn flow

1. INTRODUCTION

The principle of airlift pumping may be understood by considering the basic arrangement pictured in figure 1. A liquid tank is connected to one leg of a U tube. Air is injected near the bottom of the other leg. As a result, the fluid in this leg is lighter and rises to the top of the tube.

The airlift present, among others, the advantage of involving no moving part. However, for certain combinations of the geometrical parameters and airflow rate, they may become unstable. In this case, the flow at the riser outlet pulsates strongly, which cannot be accepted for many applications.

Small diameter (less than 40 mm) airlifts are widely used in nuclear fuel reprocessing plants. There is thus a particular need for accurate knowledge of airlift operation in this diameter range. Besides, in reprocessing plants, the stability problem is particularly acute. Indeed, the air flow regulating valves have to be kept outside the contaminated areas, which often implies the existence of long pipes between the valves and the air-injection devices. This has been shown to promote and amplify instability. Furthermore, the stability behaviour of small diameter airlifts is very complex and not readily predictable. Therefore, there is also a strong need for a detailed analysis of the stability of small diameter airlifts.

The stability problem is left aside here, and will be dealt with in a distinct article. However, the results of the stability analysis will strongly depend upon the steady-state solution. The steady state solution on its own applies to stable airlift operation, which may be characterized by the absence of low frequency (fraction of a Hertz) fluctuations of the liquid flow at the pump outlet.

Clark & Dabolt (1986) published a thorough study of the stable airlift operation, already stressing the application to nuclear fuel reprocessing. However, they did not attempt an accurate description of the frictional pressure losses in the riser, and used an approximation of the general Lockhart–Martinelli (1949) correlation. Clark & Dabolt argued that the frictional pressure losses only represented a second order contribution to the overall pressure gradient, in the airlift practical operating range. This is true for the experimental data they used, which correspond to 38 and

†Present address: Thermal-Hydraulics Laboratory, Paul-Scherrer Institute, CH-5232 Villigen-PSI, Switzerland.

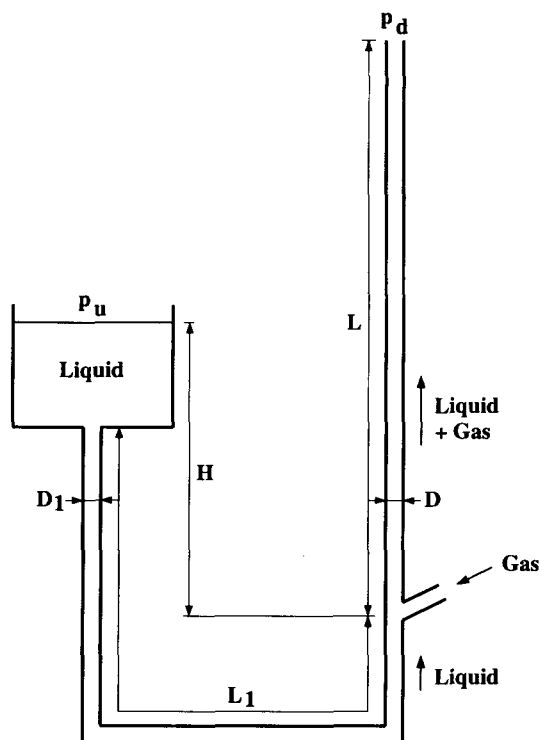


Figure 1. Typical airlift geometry. D, D_1 : internal diameters of the riser and of the liquid suction pipe, respectively; p_u, p_d : upstream and downstream pressure; $S \triangleq H/L$: submergence.

127 mm diameter airlifts. However, our experimental results, obtained in a 10 mm riser, show that the friction term becomes significant for small diameters. Airlifts having a diameter of the order of 10 mm or smaller are widely used in reprocessing plants and thus deserve a particular attention. Moreover, the error made in attempting to predict the wall friction term in small (below 40 mm) diameter risers with rough models may have the same order of magnitude than this term itself. Even if this term is relatively low, the resulting error on the pressure gradient may thus be significant. Indeed, the main flow pattern in the airlift practical operating range is slug flow, with very particular wall friction characteristics. For example, in upward slug flow, due to the contribution of the liquid films falling around the gas bubbles, the average wall shear stress may be directed upwards, in which case nonspecific friction models are obviously inappropriate.

Another specificity of small diameter airlifts relates to the gas-liquid relative velocity. This relative velocity is reduced by surface-tension effects, and, for some liquids more viscous than water, by viscous effects. The surface-tension effects have been successfully addressed by Reinemann *et al.* (1990). Beside this aspect, it is estimated here that their analysis of small diameter airlift pumps does not go far enough for the application mentioned. First, the friction model used is shown hereafter to be inadequate. In addition, quite restrictive assumptions are made. For example, there is no account of the effect of the pressure on the air density and volumetric flow rate, which limits the applicability of the model to short airlifts. The changes in momentum of the liquid, particularly in the air-injection zone, are also not accounted for.

Generally, the main shortcoming of the existing airlift models when applied to small diameter airlifts is that they overpredict the frictional pressure drop due to the lack of a slug-flow specific friction model. In many cases, the shortcoming has been concealed by the following effect. There is a strong length effect on airlift performance. For example, we experimentally found that the maximal liquid flow rate in an airlift, 20 mm in diameter, having a length-to-diameter ratio (L/D) of about 70 was almost two times lower than for a tall ($L/D > 250$) airlift (de Cachard 1989). Our experimental results show that the length effect results from the development of the two-phase flow, downstream of the air-injection zone. In the developing length, which may correspond to several hundred times the tube diameter, the frictional pressure losses are significantly higher than further

downstream. Airlift models are often compared to relatively short laboratory experiments, where the average pressure gradient is enhanced by entrance effects. Reasonably good results may then be obtained with models that would overpredict the average pressure gradient in a tall airlift. This is certainly the case, for example, for Kouremenos & Staïcos (1985), who applied a rough two-phase flow friction correlation proposed by Todoroki *et al.* (1973) to risers, 12–19 mm in diameter, with length-to-diameter ratios ranging from about 50 to 80.

In the available literature, airlift models seem to only have been compared with overall experimental results, i.e. results based on liquid vs. air flow rate measurements. This does not allow, for example, to discriminate between the gravitational and the frictional components of the pressure gradient. No account has been found of more detailed measurements performed on airlift experiments.

A new steady state model is proposed here as basis for airlift design and further stability analysis. It is focussed on small diameter (less than 40 mm), tall (length-to-diameter ratio greater than 250) airlifts. The assets of the above-mentioned models are taken up, and their reported shortcomings are addressed. The analysis is supported by a detailed experimental investigation, including pressure drop and void fraction measurements.

2. ANALYTICAL AND EXPERIMENTAL BACKGROUND

2.1. Statement of the problem

Although their operating principle remains the same, airlifts present various geometries. In particular, the geometries of the liquid and air supply pipes as well as that of the riser are adapted

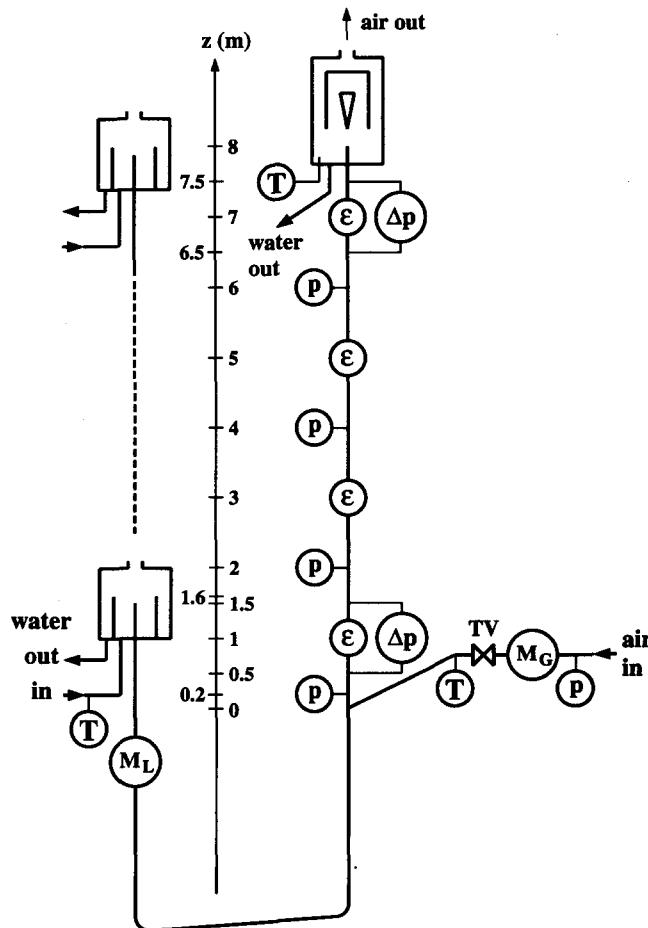


Figure 2. Experimental setup. TV: throttling valve, M_L : liquid mass flow measurement, M_G : gas mass flow measurement, T : temperature measurement, p : relative pressure measurement, Δp : differential pressure measurement, ϵ : void fraction measurement.

to each particular application. The pressure conditions prevailing upstream and downstream of the airlift are also a differentiating feature. The particular design represented in figure 1 is taken as a basis for the present analysis.

In practice, the main purpose of the design of small diameter airlifts is to be able to regulate the liquid flow rate, in a given range, by controlling the injected air flow rate. This requires the operating point, or range, first, to be stable, and then to lie in the left-hand, steep, and quasi-linear part of the liquid flow rate vs gas flow rate curve (e.g. figure 17). The optimization of the energetic efficiency is of little economical interest in this case, where, anyway, only low amounts of compressed air are used. The problem is posed here in terms of the prediction of the liquid mass flow rate M_L as a function of the air mass flow rate M_G . The geometrical parameters (H, L, L_1, D, D_1), the pressure conditions (p_u, p_d), and the fluids physical properties are given as input data to the calculations. As all the system variables are explicitly computed, secondary results such as the efficiency may easily be determined. The steady-state values of the system variables will also be used for the stability analysis which will be dealt with in a subsequent article.

2.2. Basic equations

The single phase liquid flow in the suction pipe and the two-phase flow in the riser are considered as isothermal. The main variables used for the two-phase flow characterization are the superficial velocities J_G and J_L and the void fraction ϵ . The gas and liquid mass balances give, the riser:

$$J_G = \frac{M_G}{\rho_G A} = \epsilon V_G \quad [1]$$

$$J_L = \frac{M_L}{\rho_L A} = (1 - \epsilon) V_L \quad [2]$$

where V_G and V_L denote the gas and liquid velocities, respectively, and A the riser cross-sectional area.

The pressure decrease over the riser height induces an expansion of the gas. This is accounted for, assuming that the gas behaves as an ideal gas:

$$\rho_G = \rho_{Gr} \frac{p}{p_r}, \quad [3]$$

ρ_{Gr} being the gas density at a reference pressure p_r .

The momentum balance is written for the gas-liquid mixture, neglecting the gas weight and momentum:

$$\frac{dp}{dz} = \left(\frac{dp}{dz}\right)_g + \left(\frac{dp}{dz}\right)_f + \left(\frac{dp}{dz}\right)_a \quad [4]$$

$$\left(\frac{dp}{dz}\right)_g \triangleq -\rho_L(1 - \epsilon)g \quad [5]$$

$$\left(\frac{dp}{dz}\right)_f \triangleq 4 \frac{\tau}{D} \quad [6]$$

$$\left(\frac{dp}{dz}\right)_a \triangleq -\rho_L \frac{d}{dz} [V_L^2(1 - \epsilon)] = -\rho_L J_L^2 \frac{d}{dz} \frac{1}{1 - \epsilon} \quad [7]$$

where $(dp/dz)_g$, $(dp/dz)_f$ and $(dp/dz)_a$ represent the gravity, friction and acceleration terms; z denotes the height above the air-injection tee, and τ the wall shear stress ($\tau < 0$ for upward flow near the wall).

The momentum balance is integrated between the tee and the riser outlet:

$$\int_{z=0}^{z=L} \frac{dp}{dz} dz = p_d - p_T. \quad [8]$$

The air injection pressure, p_T , is related to the pressure in the upstream water tank through Bernoulli's equation. This equation is written for the liquid between the free surface in the upstream tank and a cross section just above the air-injection tee:

$$p_T = p_u + \rho_L g H - \frac{1}{2} \rho_L \left(J_L \frac{A}{A_1} \right)^2 \left(\lambda_1 \frac{L_1}{D} + \zeta_1 \right) - \frac{1}{2} \rho_L V_{LT}^2 (1 + \zeta_c) \quad [9]$$

where A_1 denotes the liquid suction pipe cross section area, λ_1 and ζ_1 the friction factor and the sum of the singular pressure drop coefficients in the suction pipe, respectively, and ζ_c the singular pressure drop coefficient corresponding to the liquid flow contraction in the air-injection zone. Because of the lack of data we will take $\zeta_c = 0$.

The liquid mass balance [2] gives, at the tee:

$$V_{LT} = \frac{J_L}{1 - \epsilon_T} \quad [10]$$

Assuming smooth turbulent flow in the suction pipe, the friction factor λ_1 is evaluated from Blasius' formula

$$\lambda_1 = 0.316 \text{Re}^{-0.25} \quad [11]$$

ζ_1 is evaluated from classical formulas (Idel'Chik 1960), as a function of the suction pipe geometry.

For a given gas mass flow rate, the liquid mass flow rate will be found by solving [8], in which the components of the pressure gradient in the riser are expressed by [5]–[7], and the air-injection pressure p_T by [9]. Expressions for the void fraction and the frictional term in the riser, as functions of the gas and liquid superficial velocities, are required in order to close the model. Such expressions are proposed below, based both on analytical and experimental results.

2.3. Experiments

The experimental setup basically consists of an airlift of the type represented in figure 1, with a 8 m-long, 10 mm inside diameter riser. The test section and its instrumentation are schematized in figure 2. A complete description of the loop, the measuring devices, the experimental procedures, as well as of the calibration tests and the determination of the measurements uncertainties may be found in de Cachard (1989).

A constant water level is maintained in the upstream tank using a continuously fed circular weir. The tank itself can be fixed at different vertical positions, corresponding to different airlift submergences. A constant inlet air mass flow rate is insured by means of a throttling valve which is always operated with choking pressure ratios. The gas and liquid mixing takes place in a tee junction, the gas leg being 30° downwards inclined. This design corresponds to the industrial airlifts used in reprocessing plants and is imposed by maintenance reasons. The gas-liquid separator, at the riser outlet, includes a conical deflector that prevents the liquid from falling back into the riser. The separator is open to the atmosphere, as well as the upstream tank. The two tanks, the riser and the tee junction are constructed of altuglass, thus allowing observation of the flow.

The instantaneous liquid flow rate is measured by an electromagnetic flowmeter, prior to being time-averaged. The (constant) gas mass flow rate is measured by two parallel-mounted thermal flowmeters. The pressure line in the riser is determined by gage pressure transducers, and the ambient pressure is also measured. The pressure measurements are used to determine the local gas density and superficial velocity, according to [1] and [3]. The void fraction is measured at four axial locations by resistivity probes with flush-mounted electrodes. Each probe measures an instantaneous volumetric void fraction. The measurement volume is a section, about 10 mm high, of the riser. The water temperature is measured in the upstream tank feed line and in the separator. During the tests, the temperature difference between these two extreme points was less than 0.5°C. It is thus assumed that the flow is isothermal. Finally, differential pressure measurements are performed along two 1 m-long sections centered on the first ($z = 1$ m) and the last ($z = 7$ m) void fraction measurements.

The experimental setup has been used for two series of experiments. First, a systematic investigation of the void fraction and of the wall friction in the riser has been performed. Then, the overall airlift performance has been measured, for different submergences.

The test grid for the *first* experiments has been defined in terms of gas and liquid mass flow rates. The purpose was to cover the superficial velocity range of practical interest for small (up to 40 mm) diameter airlifts. The gas and liquid superficial velocities were up to 3.5 and 1.1 m/s, respectively. For these experiments, the test apparatus (figure 2) had been slightly modified. The upstream tank was by-passed, and a given water flow rate was imposed at the riser inlet by means of a pump and a throttling valve. This allowed to cover a wider liquid flow rate range than with the airlift configuration. Moreover, it prevented flow instabilities in the riser.

The void fraction was registered at a frequency of 50 Hz and time-averaged over 1 min. The frictional component of the pressure gradient is obtained by subtracting the gravitational and accelerational components from the measured total value [4]. The gravity term is deduced from the value of the void fraction [5]. The acceleration term is theoretically estimated ([46] and [47] below). It represents no more than 0.6% of the pressure gradient, in the results presented.

The *second* series of experiments consisted in registering the liquid mass flow rate as a function of the injected air mass flow rate, for different airlift submergences.

The measurement results are presented and discussed below, together with the modelling aspects.

3. EXPERIMENTAL RESULTS AND ANALYSIS

3.1. Flow patterns

An accurate prediction of the void fraction and the wall friction in the riser requires the knowledge of the two-phase flow pattern. It is generally assumed (Todoroki *et al.* 1973; Clark & Dabolt 1986; Reinemann *et al.* 1990) that this flow pattern is slug flow. Upward vertical slug flow consists of periodic, long cylindrical bubbles, surrounded by thin falling liquid films and separated by liquid slugs.

The test grid of our first experiments (forced flow) is based on the airlift-relevant gas and liquid superficial velocity range. Figure 3 shows how the test points distribute on a Brauner & Barnea (1986) flow map, which is refinement of the one proposed by Taitel *et al.* (1980). For the test points, the gas superficial velocity is taken at atmospheric pressure, i.e. the mapped flow pattern corresponds to the flow near the riser outlet.

All the experimental points lie in the slug flow and churn flow domains of the map. Churn flow differs from slug flow in that it looks more disordered. The shape of the gas bubbles is distorted,

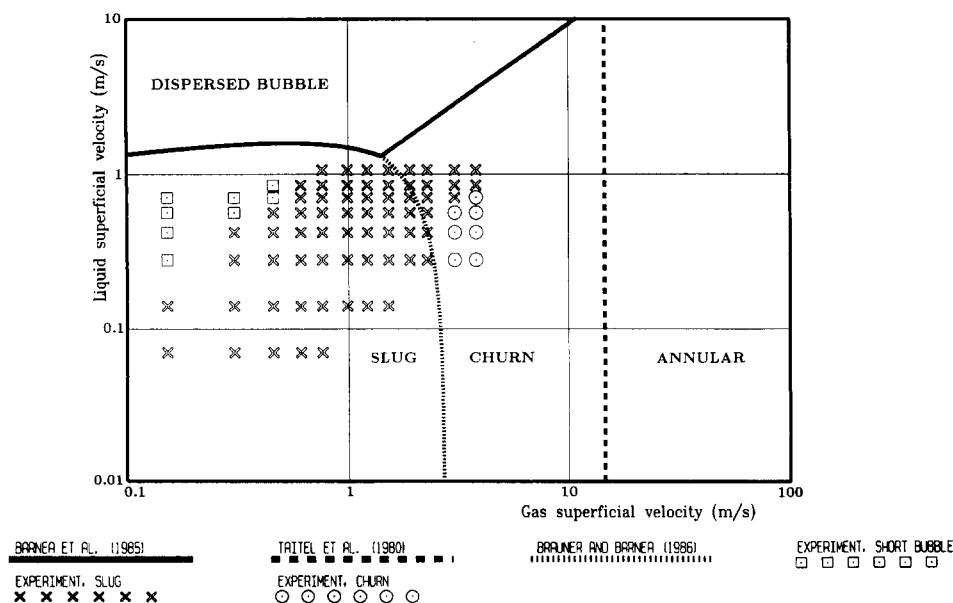


Figure 3. Distribution of the forced flow test points on a Brauner & Barnea (1986) flow map. Air–water, 20°C, 1.013 bar, $D = 10$ mm.

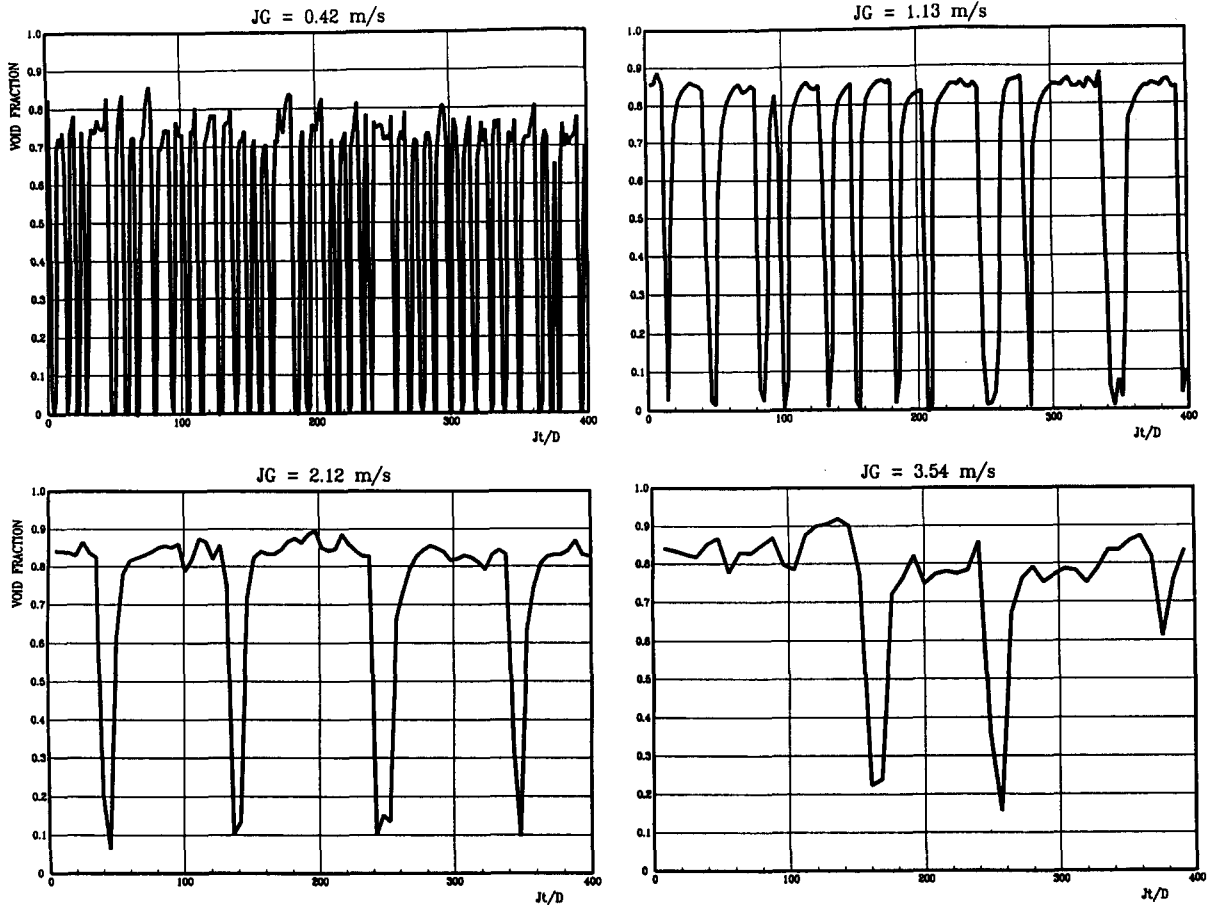


Figure 4. Instantaneous void fraction records for the middle range liquid superficial velocity ($J_L = 0.28$ m/s) and increasing gas superficial velocities.

and the liquid around the bubbles presents oscillatory motions. Liquid slugs may be observed in churn flow, but they are highly aerated.

The flow map predictions have been assessed against both visual observations and instantaneous void fraction measurements, performed at $z = 7$ m (1 m below the riser outlet). Indeed, these measurements give a good representation of the flow pattern, as may be seen in the examples displayed in figures 4–6.

In order to keep the same scale for the various gas and liquid superficial velocities, a time-space transformation has been performed: the void fraction is not plotted vs t (time), but vs Jt/D , where J is the superficial velocity of the mixture:

$$J \triangleq J_G + J_L, \quad [12]$$

and D is the pipe diameter. As J is of the same order as the propagation velocities of the flow structures, each graph roughly corresponds to the picture of a given flow length.

The void fraction acquisition frequency of 50 Hz is somewhat insufficient for this application, but it was well suited to long period acquisition, in view of averaging.

The experimental results agree well with the flow map predictions (figure 3), except for the highest gas and liquid velocities. In this case, the flow pattern is rather slug flow than the churn flow predicted, as illustrated by the instantaneous void fraction record displayed in figure 6, right. This point has already been raised by the authors themselves (Brauner & Barnea 1986, p. 161). According to these authors, slug flow in this region of the map is of special nature. Indeed, our void fraction records reveal much more aerated slugs than for lower liquid flow rates.

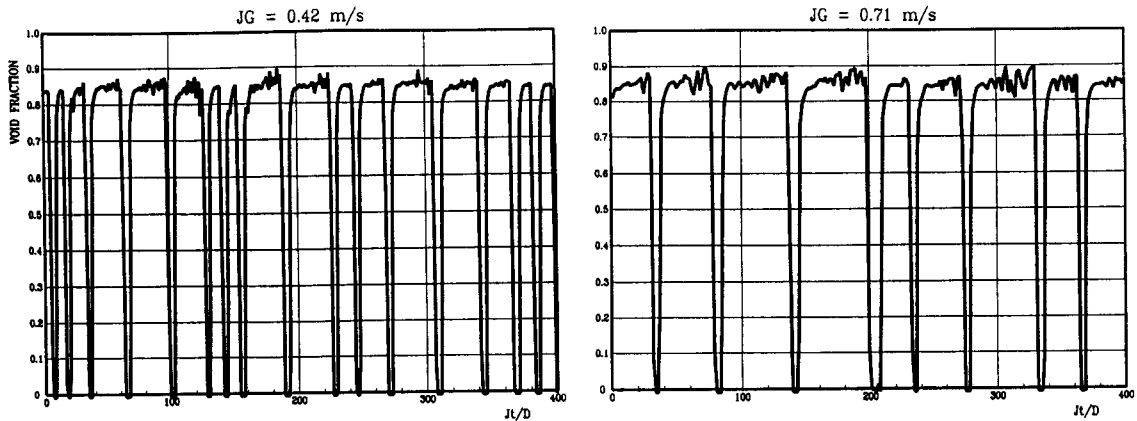


Figure 5. Instantaneous void fraction records for a low liquid superficial velocity ($J_L = 0.07$ m/s).

For lower liquid flow rates, the slug–churn transition with increasing gas flow rates is quite accurately predicted by the model. This transition is illustrated in figure 4, with, for $J_G = 0.42$ m/s, a slug flow pattern, with almost gas-free liquid slugs. For $J_G = 2.12$ m/s (corresponding to the theoretical transition on the flow-pattern map), it may be seen (figure 4), that the falling liquid films become agitated, and the liquid slugs aerated. The rapid increase of the slug void fraction near the transition is predicted by the Brauner & Barnea model, although the predicted void fraction values are larger than our measured values. Finally, the flow pattern corresponding to $J_G = 3.54$ m/s may be interpreted as churn flow.

Taitel *et al.* (1980) considered churn flow as an entry phenomenon of the slug flow pattern. It seems clear now that churn flow may exist as a developed flow pattern at high enough gas flow rates (Brauner & Barnea 1986; Jayanti & Hewitt 1992). The occurrence of churn flow in the entry region, in the case where the developed flow pattern is slug flow, is an additional effect. It has also been experienced in our 10 mm riser. Nevertheless, in this case, the churn flow length was much smaller than predicted by the Taitel *et al.* model.

Within the slug flow domain, we attempted to distinguish between a domain with long bubbles (experimental points qualified as “slug” in figure 3) and another with relatively short bullet-shaped bubbles (“short bubble” in figure 3). This discrimination will be later motivated by considerations upon the wall friction. In figure 3, experimental points have been arbitrarily qualified as “short bubble” if the most frequent bubble lengths were estimated to be lower than five times the tube diameter. The “short bubble” flow pattern would correspond, for example, to figure 6, left (visual observation would be required, here, for better understanding of the flow structure), whereas the “true” slug flow pattern is illustrated in most of the void fraction graphs presented.

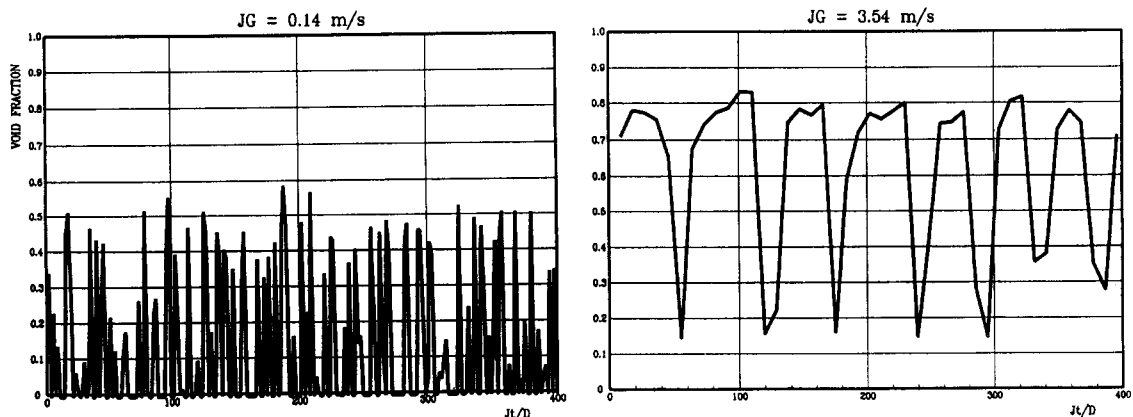


Figure 6. Instantaneous void fraction records for two high liquid superficial velocities (left: $J_L = 0.71$ m/s, right: $J_L = 1.06$ m/s).

In summary, both the flow pattern map used and the experimental results obtained indicate slug flow as the dominant flow pattern in the investigated velocity range, for air–water flow in a 10 mm riser. Churn flow is present at high gas velocities, and has to be accounted for, as the airlift operating points may lie in the slug-churn transition zone. Besides, the effect of the tube diameter on the flow pattern may be observed in the theoretical and experimental flow maps by Brauner & Barnea (1986, figures 3–5). Clearly, the above conclusions upon flow pattern remain valid for diameters up to 40 mm. In the following, specific closure laws are proposed for the slug and churn flow patterns. The void fraction and wall friction predictions are then assessed against experimental results.

3.2. Slug flow model

Sophisticated models have been developed for gas–liquid slug flow in vertical tubes, (e.g. Fernandes *et al.* 1983). In this model, steady and fully developed slug flow is described as a succession of identical unit cells. A unit cell consists of a cylindrical Taylor bubble surrounded by a falling liquid film and of a liquid slug. The complexity of the model mostly relates to the prediction of the gas content of the liquid slugs.

In our experiments, when the flow pattern was specifically slug flow, the liquid slugs were free of gas bubbles. According to Ros (1961), the condition for non-aerated liquid slugs is:

$$Bo \triangleq \frac{(\rho_L - \rho_G)gD^2}{\sigma} < 140 \tag{13}$$

where *Bo* is the Bond number, and σ is the surface tension. This corresponds, with air and water at 20°C and atmospheric pressure, to $D < 32$ mm, which is approximately the diameter range of interest in this study. Thus, in the analysis, a zero void fraction is assumed in the liquid slugs. Under this assumption, the unit cell of the above-mentioned model reduces to the situation sketched in figure 7.

According to the cellular model, in a fixed cross section, the Taylor bubbles and the liquid slugs follow one another at regular intervals. The steady state values to be used in the airlift basic equations ([1]–[11]) are the averaged values over one period of the phenomenon, i.e. over the transit time of one unit cell. The closure laws related to the slug flow regime will be derived, first, by relating the instantaneous slug flow variables to the average gas and liquid superficial velocities, and then, by deducing the average gravitational, frictional and accelerational components of the pressure gradient from the instantaneous variables.

The fraction of the unit cell transit time corresponding to the Taylor bubble is:

$$\beta \triangleq \frac{l_B}{l} \tag{14}$$

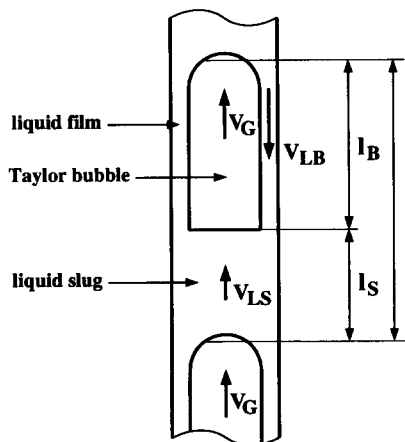


Figure 7. Slug flow unit cell. *l*: unit cell length; *l_B*, *l_S*: Taylor bubble and liquid slug length, respectively; *V_G*: Taylor bubble rise velocity; *V_{LB}* (<0), *V_{LS}*: mean liquid velocity in the falling film and in the slug, respectively.

On the scale of the unit cell, the gas is assumed to be incompressible. For the gas, the liquid and the mixture, the instantaneous continuity equations read

$$\frac{\partial}{\partial t} \epsilon + \frac{\partial}{\partial z} (\epsilon V_G) = 0 \tag{15}$$

$$\frac{\partial}{\partial t} (1 - \epsilon) + \frac{\partial}{\partial z} [(1 - \epsilon) V_L] = 0 \tag{16}$$

$$\frac{\partial}{\partial z} [\epsilon V_G + (1 - \epsilon) V_L] = 0 \tag{17}$$

where the slug flow instantaneous variables are underlined>.

Equations [15] and [16] are cell-averaged and integrated, under the assumption of steady average flow:

$$\langle \epsilon V_G \rangle = J_G \tag{18}$$

$$\langle (1 - \epsilon) V_L \rangle = J_L \tag{19}$$

where the cell-averaging operator is denoted by $\langle \rangle$.

Specifying the instantaneous slug flow variables, according to figure 7, leads to:

$$\beta \epsilon_B V_G = J_G \tag{20}$$

$$(1 - \beta) V_{LS} + \beta(1 - \epsilon_B) V_{LB} = J_L \tag{21}$$

where ϵ_B denotes the void fraction in the Taylor bubble zone.

Integration of [17] gives

$$\epsilon V_G + (1 - \epsilon) V_L = \text{constant} = J. \tag{22}$$

Specifying the slug flow variables, first for the Taylor bubble zone, and then for the liquid slug, gives:

$$\epsilon_B V_G + (1 - \epsilon_B) V_{LB} = V_{LS} = J. \tag{23}$$

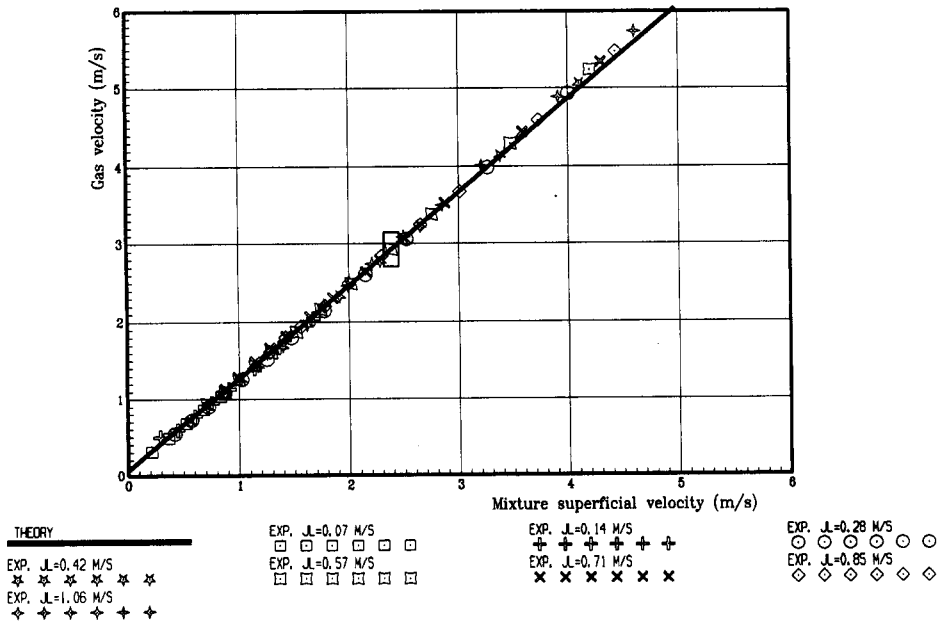


Figure 8. Average void fraction: representation of Zuber & Findlay. Comparison of experimental and predicted values of $V_G = J_G/\epsilon$, at 7 m elevation, for various values of the liquid superficial velocity J_L (□: uncertainty bands).

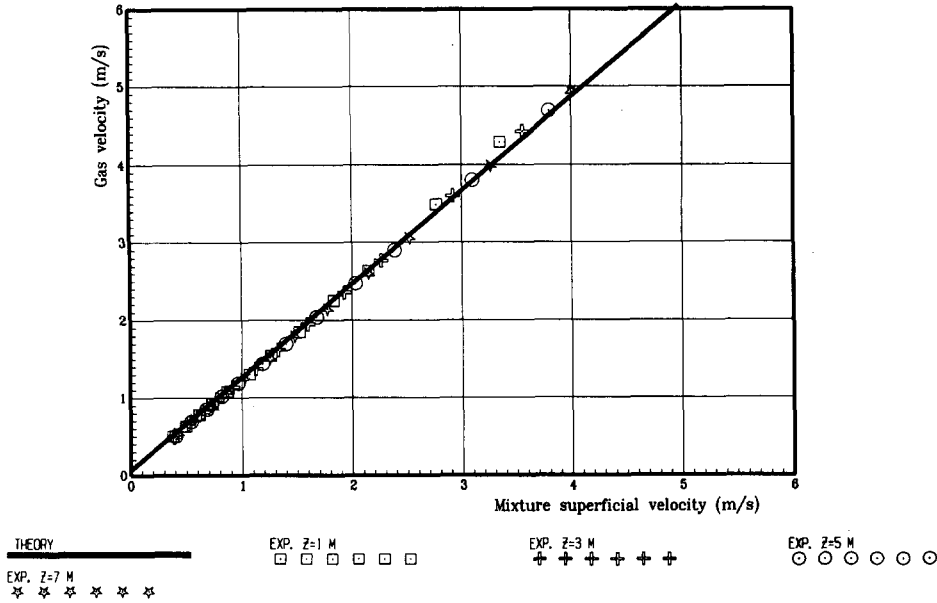


Figure 9. Average void fraction: representation of Zuber & Findlay. Comparison of experimental and predicted values for a middle range liquid superficial velocity ($J_L = 0.28$ m/s), and various elevations.

The cellular slug flow model is complemented with expressions for the Taylor bubble and the falling film velocities. The approximation of a fully developed liquid flow is made for the film, as well as for the slug.

For the *Taylor bubble* velocity, the expression proposed by Nicklin *et al.* (1962), and widely used since, is retained:

$$V_G = C_0 J + V_0 \tag{24}$$

where C_0 represents the velocity profile coefficient in the liquid slug, and is given for turbulent flow by:

$$C_0 = 1.2 \tag{25}$$

and V_0 represents the rise velocity of a Taylor bubble in stagnant liquid. The original expression for V_0 in [24] has been modified to account for interfacial and viscous forces. Indeed, according to White & Beardmore (1962), surface tension effects become significant if

$$Bo < 70 \tag{26}$$

whereas, for viscous effects, the condition is:

$$(N_f)^2 \triangleq \frac{\rho_L(\rho_L - \rho_G)gD^3}{\mu_L^2} < 3.10^5. \tag{27}$$

The first condition is fulfilled, for air and water at atmospheric pressure and 20°C, when $D < 23$ mm. The second condition is not reached for water, but it is for some more viscous fluids.

The following approximation of White and Beardmore's (1962) general correlation, recommended by Wallis (1969, p. 290), is used:

$$V_0 = \Gamma(gD)^{1/2} \tag{28}$$

$$\Gamma = 0.345(1 - e^{-0.01N_f/0.345})[1 - e^{(3.37 - Bo)/m}] \tag{29}$$

$$m = 10 \text{ when } N_f > 250 \tag{30}$$

$$m = 69(N_f)^{-0.35} \text{ when } 18 < N_f < 250 \tag{31}$$

$$m = 25 \text{ when } N_f < 18. \tag{32}$$

It should be pointed out that substituting in [24] an expression of V_0 corrected for viscous and interfacial effects does not account for their interactions with the velocity profile effect.

The *liquid film* around the Taylor bubble is modelled as a thin film falling, without interfacial shear stress, inside a vertical cylinder. For laminar flow, the film thickness, δ , is related to the mean velocity V_{LB} by Nusselt's relation:

$$\delta \left(\frac{g}{v_L^2} \right)^{1/3} = (3 \text{Re}_F)^{1/3} \tag{33}$$

where Re_F is the Reynolds number of the film, defined by:

$$\text{Re}_F \triangleq -V_{LB} \frac{\delta}{v_L} \quad (V_{LB} < 0). \tag{34}$$

For turbulent flow, according to Belkin *et al.* (1959) and Wallis (1969, p. 333),

$$\delta \left(\frac{g}{v_L^2} \right)^{1/3} = 0.159 \text{Re}_F^{2/3}. \tag{35}$$

These two relations fit together for $\text{Re}_F \simeq 750$. Substituting definitions [34] in [33] and [35] gives:

$$V_{LB} = -0.333 g \frac{\delta^2}{v_L} \quad (\text{Re}_F < 750) \tag{36}$$

$$V_{LB} = -15.8 (g\delta)^{1/2} \quad (\text{Re}_F > 750). \tag{37}$$

The geometrical relation between the film thickness and the void fraction is:

$$\delta = \frac{D}{2} (1 - \epsilon_B^{1/2}) \tag{38}$$

which gives

$$V_{LB} = -0.333 \left(\frac{gD^2}{v_L} \right) (1 - \epsilon_B^{1/2})^2 \quad (\text{Re}_F < 750) \tag{39}$$

$$V_{LB} = -11.2 [gD(1 - \epsilon_B^{1/2})]^{1/2} \quad (\text{Re}_F > 750). \tag{40}$$

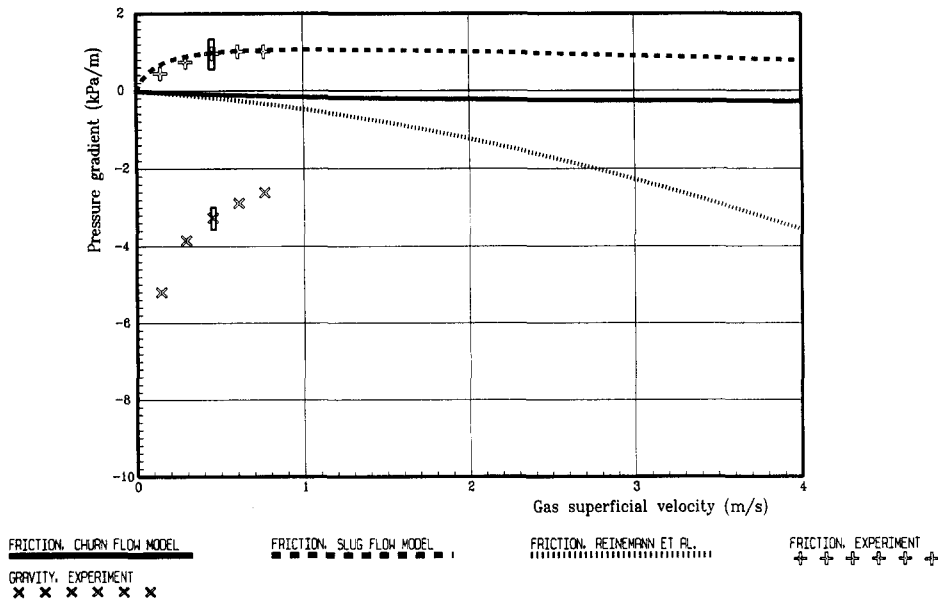


Figure 10. Frictional and gravitational components of the pressure gradient for $J_L = 0.07$ m/s. Comparison between experimental values of the friction term (\square : uncertainty bands), and values predicted by the models proposed for churn and slug flow and by the model of Reinemann *et al.* (1990).

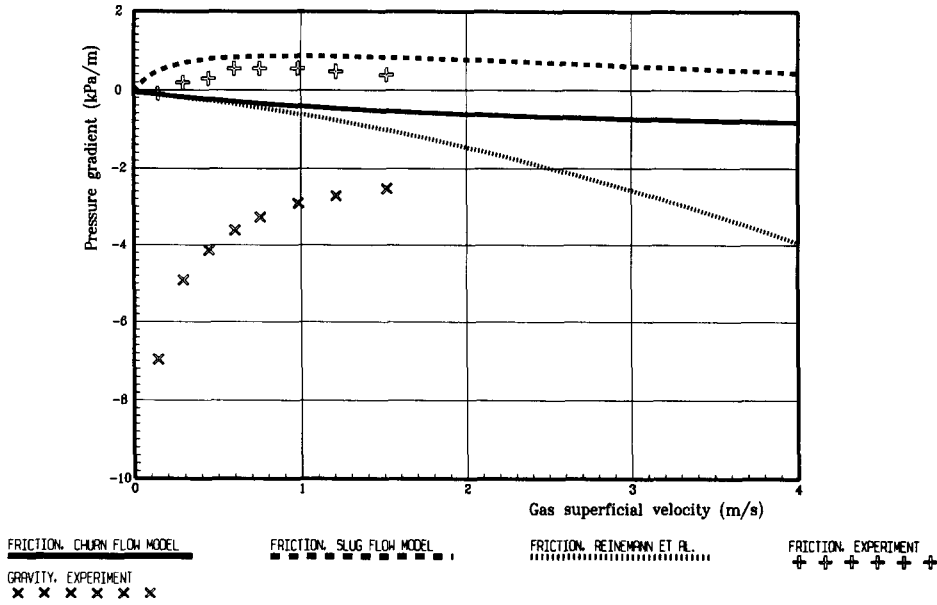


Figure 11. Frictional and gravitational components of the pressure gradient for $J_L = 0.14$ m/s.

In summary, the slug flow parameters $V_G, V_{LB}, V_{LS}, \epsilon_B, \beta$ can be computed from the superficial velocities J_G, J_L (or $J = J_G + J_L$) with the following set of equations:

$$V_G = 1.2J + V_0 \tag{24}$$

$$\epsilon_B V_G + (1 - \epsilon_B)V_{LB} = V_{LS} = J \tag{23}$$

$$V_{LB} = f(\epsilon_B) \tag{39} \text{ or } [40]$$

$$\beta \epsilon_B V_G = J_G \tag{20}$$

where V_0 is computed from [28]–[32] (V_0 is a constant related to the fluid properties and the pipe diameter).

According to [1] and [24], the average void fraction may be expressed by:

$$\epsilon = \frac{J_G}{V_G} = \frac{J_G}{C_0 J + V_0} \tag{41}$$

Thus, the model presented agrees with the expression of Zuber & Findlay (1965). $C_0 (= 1.2)$ and V_0 ([28]–[32]) may be interpreted as the distribution parameter and the weighted average drift velocity for slug flow.

The gravitational and frictional components of the pressure gradient are predicted using Wallis' (1969, pp. 294, 295) analysis. According to the cellular slug flow model, the average gravitational component ([5]) is:

$$\left(\frac{dp}{dz}\right)_g = -\rho_L g [(1 - \beta) + \beta(1 - \epsilon_B)]. \tag{42}$$

The two terms of the sum account for the liquid slug and the falling film contributions, respectively.

The friction term for the liquid slug is evaluated on the basis of a fully developed flow of velocity J :

$$\left(\frac{dp}{dz}\right)_{fs} = -\frac{\lambda_J \rho_L J^2}{2D} \tag{43}$$

where the friction factor λ_J is evaluated from Blasius' formula ([11]), with a Reynolds number based on J .

In the Taylor bubble zone, once the liquid film is fully developed, its weight is fully balanced by the wall friction force. The friction term is thus the opposite of the gravity term:

$$\left(\frac{dp}{dz}\right)_{fB} = \rho_L g (1 - \epsilon_B). \quad [44]$$

The average frictional component is:

$$\left(\frac{dp}{dz}\right)_f = (1 - \beta) \left(\frac{dp}{dz}\right)_{fB} + \beta \left(\frac{dp}{dz}\right)_{fB}. \quad [45]$$

The model used does not account for the transition between the rising liquid slug and the falling liquid film, i.e the liquid flow around the Taylor bubble nose. As shown by Barnea (1990), this leads to a slight underprediction of the frictional pressure losses in slug flow. However, the resulting error is much smaller than the difference between slug and churn flow (figures 10–14, below), which is the main topic of this work.

The accelerational component, which only represents a small contribution, is estimated by using the average flow variables ([7]). Substituting the void fraction expression ([41]) and the ideal gas law ([3]) in this equation leads, after some algebra, to

$$\frac{dp}{dz} = \alpha \left[\left(\frac{dp}{dz}\right)_g + \left(\frac{dp}{dz}\right)_f \right] \quad [46]$$

with the following expression of the acceleration correction factor α :

$$\alpha = \left[1 - \rho_L J_L^2 \frac{J_G (C_0 J_L + V_0)}{p [(C_0 - 1) J_G + C_0 J_L + V_0]^2} \right]^{-1}. \quad [47]$$

3.3. Churn flow model

The well defined structure of slug flow can be easily analysed. On the contrary, the chaotic nature of churn flow requires more empirical considerations for the void fraction and wall friction predictions.

According to Brauner & Barnea (1986), the slug-churn flow transition is related to an increase in the mixture superficial velocity J . The influence of the slug-churn flow transition on the void fraction may thus be characterized by using the variable J . The influence of J on the distribution parameter C_0 and the drift velocity V_0 may be observed in Zuber & Findlay (1965, figures 8 and

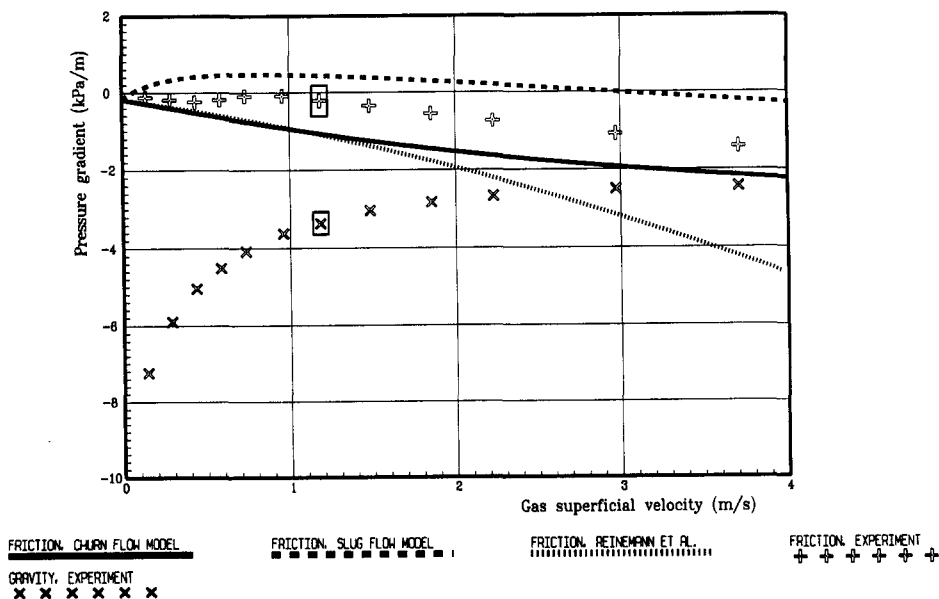


Figure 12. Frictional and gravitational components of the pressure gradient for $J_L = 0.28$ m/s.

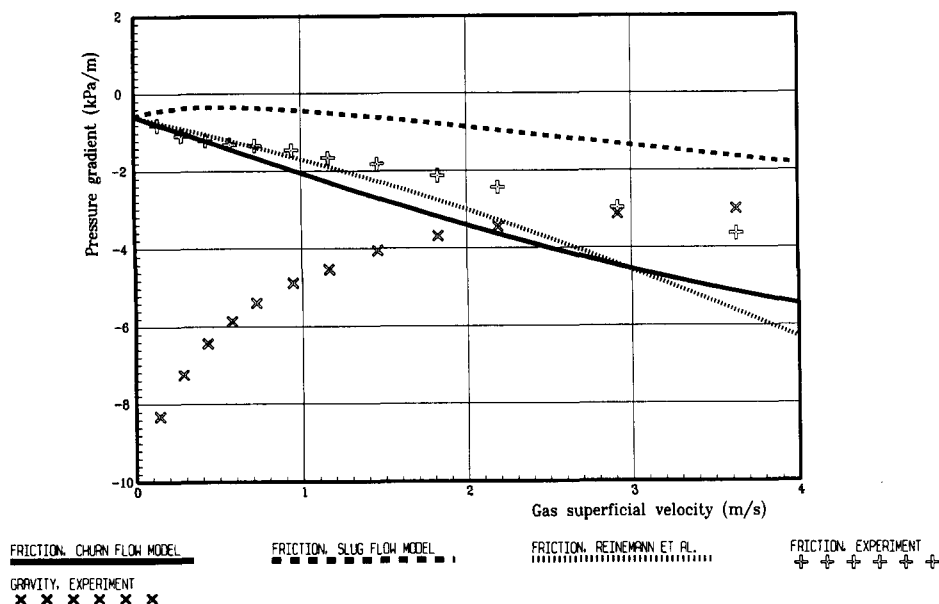


Figure 13. Frictional and gravitational components of the pressure gradient for $J_L = 0.57$ m/s.

11). For air–water mixtures at nearly atmospheric pressure, the distribution parameter C_0 and the drift velocity V_0 appear to remain constant up to a value of the mixture superficial velocity greater than 7 m/s. This value is still within the presumed churn flow domain (figure 3), but beyond the airlift-relevant range. Therefore, the subsequent evolution of C_0 and V_0 has not to be accounted for. Thus, the average void fraction in churn flow is predicted by the same relations as for slug flow ([41], [25], [28]–[32]).

A specific model for wall friction in churn flow is not yet available. The model proposed above for the instantaneous wall shear stress in slug flow is not suitable for churn flow. Indeed, in slug flow, the flow in the vicinity of the wall is very particular, with the alternance of rising liquid slugs and fast falling films. In churn flow, these particularities are not found. Counter-current flow may occur, but at lower velocities and over shorter lengths. The methods used for vertical upward cocurrent annular flow analysis (like in Hewitt & Hall-Taylor 1970) seem more suitable, but, according to Govan *et al.* (1991), they still fail in predicting the mean wall shear stress in churn flow. Moreover, the development of a realistic model for churn flow is qualified by Govan *et al.* as “particularly challenging”.

Assuming that the frictional pressure drop in churn flow is the same as in a turbulent single phase liquid flow of velocity V_L (average liquid velocity in the two-phase flow) we use:

$$\left(\frac{dp}{dz}\right)_f = -\lambda \rho_L \frac{V_L^2}{2D} \quad [48]$$

where the friction factor λ is evaluated from Blasius’ formula [11], with a Reynolds number based on V_L .

Equation [48] represents a variant of the result of the simple separated flow analysis neglecting gravity effects on the liquid velocity profile (Wallis 1969, pp. 323–329). The difference is that the friction factor λ is based here on V_L instead of J_L (liquid superficial velocity), which leads to lower values of λ . A relation equivalent to [48] is used by Todoroki *et al.* (1973) in their airlift model.

The prediction of the acceleration term in churn flow is based, as in slug flow, on [46] and [47].

3.4. Void fraction

The theoretical description of the void fraction ([41], [25], [28]–[32]) was assessed against the results of our forced flow tests (test grid in figure 3). The average void fraction was analysed using the representation of Zuber & Findlay (1965): average gas velocity ($V_G = J_G/\epsilon$) vs mixture superficial velocity ($J = J_G + J_L$). In these coordinates, the model used is represented by a straight

line whose slope and intercept are the distribution parameter ($C_0 = 1.2$) and the drift velocity V_0 ([28]–[32]).

The results are presented in figures 8 and 9. In figure 8, the experimental values were obtained from the last conductivity probe (7 m above the air-injection tee), for all of the tests performed. In figure 9, the results obtained at the various measurement levels for a middle-range liquid velocity and all gas velocities are displayed.

The agreement between theory and experiment is excellent, which confirms the validity of the drift flux model for void fraction prediction, and the value $C_0 = 1.2$ for slug flow. The expression used for V_0 , and, in particular, the decrease in V_0 , due to surface-tension effects, in a small diameter pipe, are also confirmed.

The slug–churn flow transition proves to have little influence on the drift flux parameters, as assumed in the analysis: the experimental points obtained for the highest superficial velocities, which correspond to the churn flow pattern, are still well predicted by the slug flow void fraction model. Finally, the effects of the flow development over large distances downstream of the mixing zone, i.e. the evolution from churn flow or slug flow with short gas bubbles towards developed slug flow, also show no influence on the void fraction: the results obtained at the various elevations do not differ (figure 9).

3.5. Wall fraction

The experimental values of the frictional pressure drop at 7 m elevation are compared with the predictive models proposed for slug and churn flow. A sample of the results is displayed in figures 10–14. The gravity term is also displayed for comparison, as well as the values predicted by the model of Reinemann *et al.* (1990).

An overall examination of the results shows that the curves given by the slug and churn flow models surround the experimental data, and roughly follow their main trends. A deeper examination reveals some trends of the experimental results to be closer to one theoretical curve or to another. Referring to the flow pattern analysis in section 3.1, clearly shows that these trends may be correlated with the flow pattern. As the flow pattern evolves from “ideal” slug flow, i.e. a regular geometry with long Taylor bubbles, smooth falling liquid films and gas-free liquid slugs, towards irregular slug flow and churn flow, the experimental points tend to move from the neighbouring of the theoretical slug flow curve towards the churn flow curve. There is an additional effect: the “short bubble” flow pattern, described in section 3.1, is responsible for comparatively large values of the frictional pressure drop at low gas velocities. This effect was already pointed

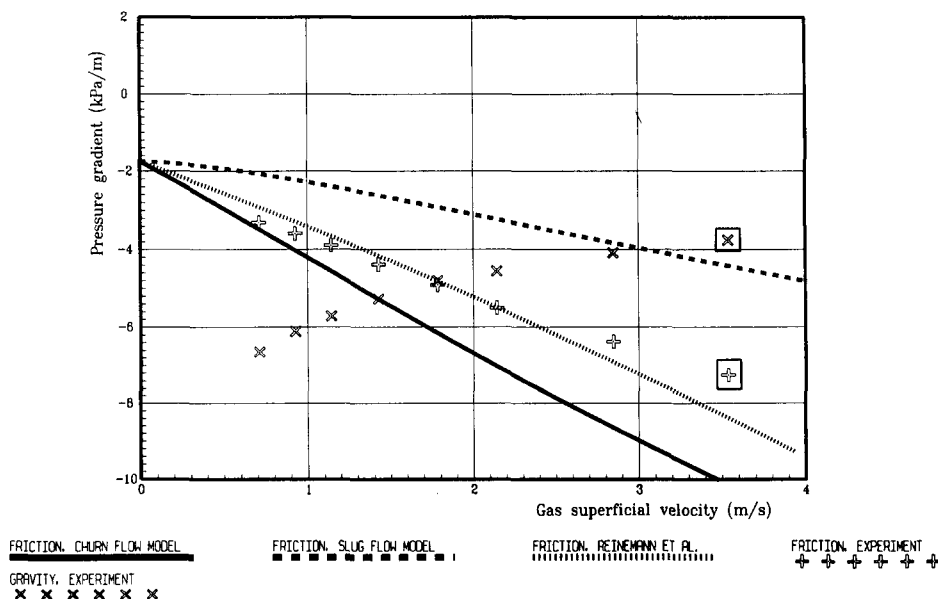


Figure 14. Frictional and gravitational components of the pressure gradient for $J_L = 1.06$ m/s.

Table 1. Interpolation coefficient for wall friction prediction (data base for C_{churn} in [49])

$\log_{10}(J_L^*)$	$\log_{10}(J_G^*)$							
	-0.8	-0.6	-0.4	-0.2	0.0	0.2	0.4	0.6
-1.0	0.424	0.330	0.194	0.056	0.051	0.152	0.280	0.386
-0.8	0.497	0.533	0.467	0.259	0.166	0.228	0.297	0.390
-0.6	0.548	0.651	0.622	0.480	0.288	0.325	0.395	0.475
-0.4	0.672	0.759	0.796	0.709	0.449	0.450	0.498	0.565
-0.2	0.900	1.063	1.023	0.901	0.657	0.599	0.569	0.578
-0.0	0.925	1.133	1.283	1.179	0.864	0.730	0.600	0.520

out by Nakoryakov *et al.* (1986, p. 345). It may be observed, for example, in figure 12, where the two first (left) experimental points correspond to the short bubble flow pattern. For the four subsequent points, a transition towards "true" (however irregular in some extent) slug flow occurs, and then, as the gas superficial velocity further increases, there is a transition towards churn flow.

The model of Reinemann *et al.* (1990), based on the slug flow pattern, only considers the contribution of the liquid slugs to the wall friction. The opposite contribution of the falling liquid films is neglected. The liquid volume contained in the films is also neglected, which leads to an overestimation of the liquid slug lengths. This results into a strong overestimation of the frictional pressure drop when the flow pattern is close to "ideal" slug flow. When the flow pattern is "short bubble" flow, as for the left parts of figures 12 and 13, or highly aerated slug flow, as for figure 14, the frictional pressure drop, being comparatively high, is no more overpredicted by the model.

In an attempt to account in a semi-empirical way for the progressive and complex transition from slug to churn flow, the airlift model that we propose uses a linear combination of the values predicted by the slug and churn flow models:

$$\left(\frac{dp}{dz}\right)_f = (1 - C_{\text{churn}}) \left(\frac{dp}{dz}\right)_{f,\text{slug}} + C_{\text{churn}} \left(\frac{dp}{dz}\right)_{f,\text{churn}} \quad [49]$$

The coefficient C_{churn} has been mapped, based on our experimental results, in the same way as the flow pattern in figure 3. However, the flow pattern map, based on the J_G, J_L coordinates, depends upon the pipe diameter and the fluid physical properties. As our C_{churn} map is intended to be used, without change, in a certain diameter range and for different fluids, these coordinates are not convenient. The main phenomenon that has to be accounted for by the C_{churn} map is the

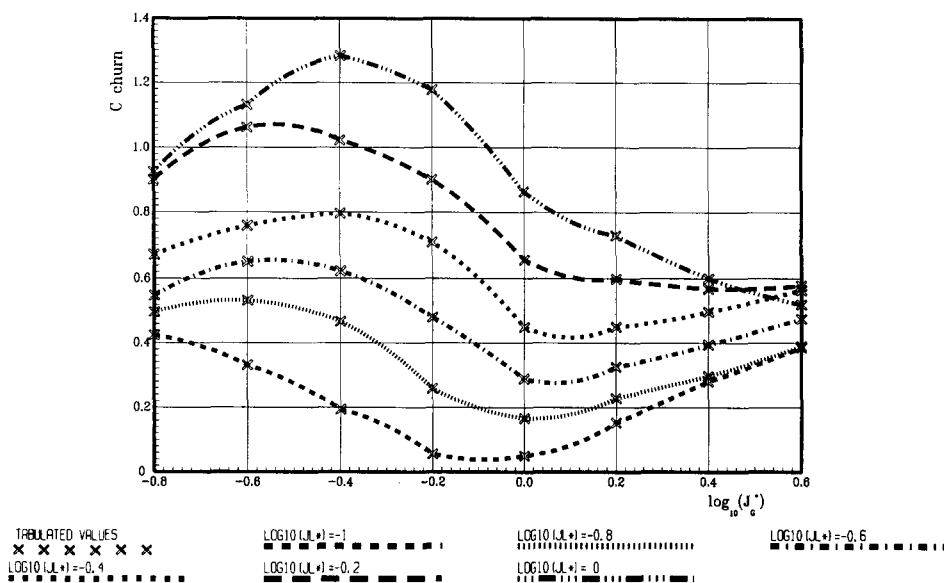


Figure 15. Interpolation coefficient for wall friction prediction (C_{churn} in [49]) as a function of $\log_{10}(J_G^*)$, with $\log_{10}(J_L^*)$ as a parameter. J_G^* and J_L^* are defined by [50] and [51].

transition from “ideal” slug flow towards irregular slug flow and churn flow. This transition has been shown to be fairly well predicted by the Brauner & Barnea (1986, [1]) criterion. This criterion is invariant in the J_G^*, J_L^* coordinates, defined as:

$$J_G^* \triangleq J_G K^{5/[2(3-n)]} \tag{50}$$

$$J_L^* \triangleq J_L K^{5/[2(3-n)]} \tag{51}$$

with

$$K \triangleq 2 \left[\frac{0.4\sigma}{(\rho_L - \rho_G)g} \right]^{1/2} \left(\frac{\rho_L}{\sigma} \right)^{3/5} \left[\frac{2}{D} C_L \left(\frac{D}{v_L} \right)^{-n} \right]^{2/5} \tag{52}$$

$$C_L = 0.046 \tag{53}$$

$$n = 0.2. \tag{54}$$

Thus, our C_{churn} map has been based on these coordinates. The value of C_{churn} has been deduced from the experimental value of the frictional pressure drop, for each test point. The results have been smoothed, and interpolated on a rectangular grid in $\log_{10}(J_G^*), \log_{10}(J_L^*)$. The resulting table (table 1) is used as a data base for quadratic interpolation in the predictive model. When $\log_{10}(J_G^*)$

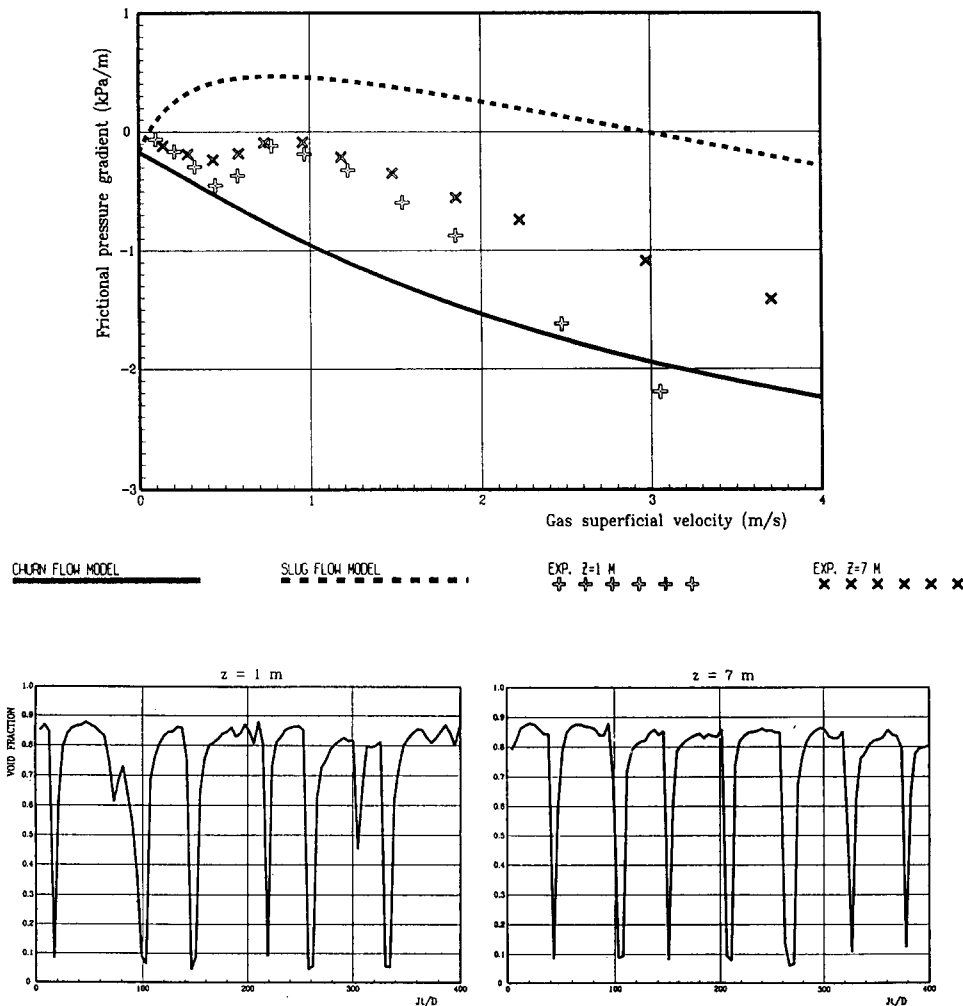


Figure 16. Entrance effects on wall friction. Comparison between experimental values of the frictional pressure gradient at 1 m and 7 m elevation, for a middle range liquid superficial velocity ($J_L = 0.28$ m/s). Instantaneous void fraction records for $J_G = 1.77$ m/s are also presented, to illustrate flow pattern development.

or $\log_{10}(J_L^*)$ is below the first tabulated value, the value of C_{churn} corresponding to the first tabulated value is used.

The values in table 1 are presented in a graphical form in figure 15. This figure must be considered with caution. Indeed, in the left part of this figure (which, in fact, is dilated by the logarithmic scale), at low gas velocities, the dominant underlying phenomena are the “short bubble” flow pattern and its transition forms (figure 3). The influence of the slug-churn transition, which has been emphasized, and which results in an increase in C_{churn} , mainly appears in the right part of the figure, i.e. at relatively high gas velocities.

The following remarks should be made here:

- The degree of relevance of each of the forced flow test points to airlift operation is not the same. The combination of a low gas velocity and a large liquid velocity is rather unrealistic, if the liquid flow is driven by the gas flow.
- At low gas velocities, and provided the liquid velocity is not too high, the pressure gradient is dominated by the gravity term, as may be seen in figures 10–14. The relative precision of the frictional term prediction has thus little influence on the overall result.

Therefore, for the present application, the relatively high gas velocities are of primary interest, and the slug-churn transition is the main issue, the “short bubble” flow pattern representing only a secondary one.

Finally, the influence of the flow development downstream from the mixing zone on the wall friction should be pointed out. This influence is illustrated in figure 16, where some results obtained 1 m and 7 m downstream from the air-injection tee are compared. Clearly, at high gas flow rates, the frictional pressure drop is much higher at 1 m elevation. The entrance effects affect the flow pattern, as may be seen in the instantaneous void fraction records obtained, at the two elevations, for the same values of the gas and liquid superficial velocities (figure 16): the flow is more agitated at 1 m elevation.

As the entrance effects are not accounted for by the present model, this model would lose in precision if applied to short (typically, length-to-diameter ratios less than 250) airlifts.

4. MODEL ASSESSMENT

The predictive model that we propose consists of the basic equations given in section 2.2 and the closure equations presented in sections 3.2 and 3.3 for the slug and churn flow patterns, together with the interpolation procedure described in section 3.5. This model has been assessed against the results of 20 airlifts from the nuclear reprocessing field. These results are proprietary, but, as examples, the model predictions are compared hereafter with the experimental results listed in table 2.

The agreement between the model and our own experimental results is excellent, as may be seen in figure 17. This was expected, because some measurements performed on the same setup have been used to adjust the friction model. However, the adjustment has not been based on the airlift experiments themselves (table 2), but on pressure drop and void fraction measurements performed during distinct forced flow experiments (figure 3). Thus, the accuracy of the overall airlift performances predictions strongly supports both the validity of the basic equations proposed, and

Table 2. Data used in the calculations (geometrical parameters defined in figure 1)

Experiment	Present work		Reinemann <i>et al.</i> (1990)			
Fluids			air water			
Pressure			1.013 bar (outlet)			
Temperature			20°C			
D (mm)	10				3.18	
D_1 (mm)	9.2				3.18	
L (m)	8				1.8	
Submergence (%)	50	70	57	71	85	98
L_1	9.14	10.62			0	
ζ_1 [9]	3.26	3.56			0.5	

the quality of the pressure drop measurements performed. Moreover, the void fraction results seem quite reliable, particularly as they are quite coherent with numerous and acknowledged previous results. Consequently, the wall friction results, which represent the difference between the total pressure drop and the gravitational component, should be quite reliable too.

Figure 17 also shows the predictions of the model of Reinemann *et al.* (1990) for our experimental conditions. A correction has been made to account for the pressure drop in the liquid suction pipe, which was not included in the model. Besides, for the drift flux model, the air density and volumetric flow rate have been taken at the average pressure between the air injection and the outlet (the model does not account for gas expansion effects).

Due to the already mentioned overestimation of the frictional pressure drop, the model of Reinemann *et al.* strongly underestimates the liquid flow rate at high gas flow rates. For the lowest submergence, which corresponds to comparatively small liquid flow rates and a flow pattern close to "ideal" slug flow, the liquid flow rate is also underpredicted at low gas flow rates.

The present model also predicts the performance of very small diameter airlifts well, as may be seen in figure 18. For these experiments, performed in a 3 mm riser by Reinemann *et al.*, the prediction is rather better than with these author's model.

In this case, for a very small diameter and high submergences, the predictions of the model of Reinemann *et al.* and of the present model are relatively close, although the friction models used are quite different. In order to understand this, the numerical values involved in the calculations have been examined in more detail. For these data, the present model works in a different domain of the variables J_G^* and J_L^* (the modified gas and liquid superficial velocities in [50] and [51]) than for our own data. The value of J_L^* corresponding to a given J_G^* is significantly higher in this case. The model, according to figure 15, uses a higher value of the interpolation coefficient C_{churn} , and, according to [49], comes closer to the churn flow model, which predicts comparatively high values of the frictional pressure drop.

In other words, and according to the considerations developed above upon flow pattern and wall friction, the experimental data of Reinemann *et al.* would correspond to "short bubble" and "agitated" slug flow. For these patterns, the frictional pressure drop is relatively high, and the friction model of Reinemann *et al.* does not overpredict it, as it does for regular slug flow.

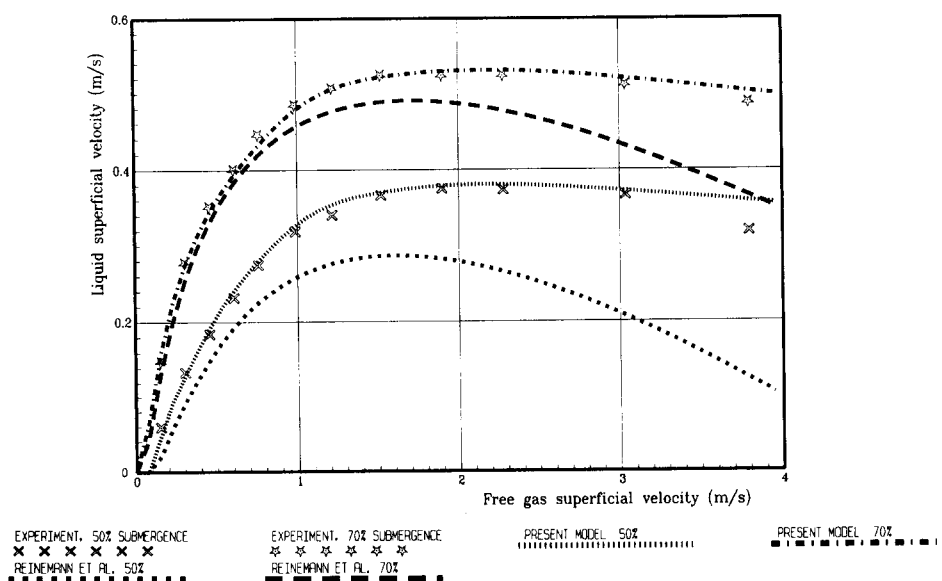


Figure 17. Airlift pumping performance: present experiments ($D = 10$ mm). Comparison between experimental values of the liquid superficial velocity, and values predicted by the present model, and by the model of Reinemann *et al.* (1990).

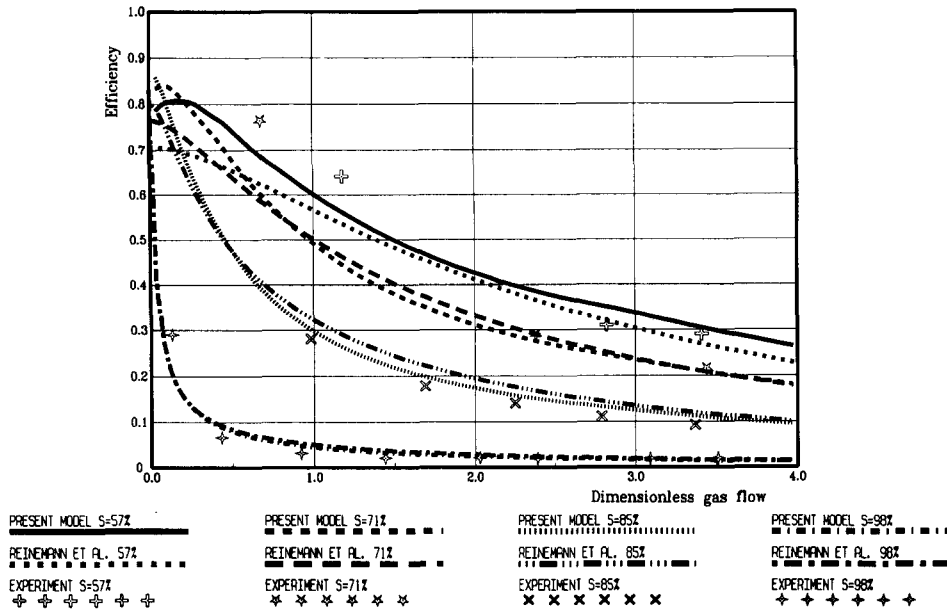


Figure 18. Airlift pumping performance: experiments of Reinemann *et al.* ($D = 3$ mm) Comparison between experimental values of the pumping efficiency, and values predicted by the present model, and by the model of Reinemann *et al.* (1990), the efficiency n , and the dimensionless liquid and gas flows Q'_L and Q'_G are defined as: $n \triangleq Q'_L(1 - S)/(Q'_G S)$, $Q'_L \triangleq J_L/(\mathbf{g}D)^{1/2}$, and $Q'_G \triangleq J_G/(\mathbf{g}D)^{1/2}$, J_L and J_G being the liquid and gas superficial velocities (taken at the average pressure), and S the airlift submergence.

5. CONCLUSION

The dominant flow pattern in the practical operating range of small diameter airlifts is slug flow. More precisely, within this flow pattern, three classes may be distinguished: regular, agitated and “short bubble” slug flow. As the gas velocity is increased, there is a transition towards churn flow.

The void fraction and thus the gravitational component of the pressure gradient in the riser, seems quite insensitive to these changes in flow pattern. In the airlift model proposed, the void fraction is predicted, by the drift-flux model, with a single value of the distribution parameter, and a single expression for the drift velocity (accounting for surface tension and viscosity effects).

The frictional component often represents a significant contribution to the pressure gradient in the riser. Our experimental results confirm the very particular nature of wall friction in slug flow, with a possible sign reversal. The friction is sensitive to the changes in flow pattern, which have thus to be accounted if the prediction is to be accurate.

“Ideal” slug flow and churn flow may be considered as two limiting cases for the flow patterns encountered in actual practice. The airlift model proposed uses a linear combination of models describing wall friction in slug and churn flow. These two models are based on the general literature on two-phase flow. The particular structure of slug flow is accounted for by a cellular model. The weighting coefficient between the two models has been empirically correlated, with the position of the airlift operating point on a flow pattern map. The results of accurate and carefully checked measurements, including void fraction measurements, have been used for this correlation.

The accelerational component only represents a very small contribution to the pressure gradient, except in the air-injection zone, where it may become meaningful at high void fractions. Attention has been paid to this term in the present airlift model. In addition, integration of the airlift operating equation along the riser height allows large variations in the gas density and velocity to be accounted for. As a result, the behaviour of high airlifts can also be predicted.

The experiments performed allowed to clearly identify the cause of the favourable effect of the riser length on airlift performance, at constant submergence, as pointed out in the introduction. This length effect could not be quantified but on an empirical basis.

The steady-state model proposed represents an accurate analysis tool for the design of small diameter (up to 40 mm), tall (length-to-diameter ratio greater than 250) airlifts. Not only the airlift overall performance is accurately predicted, but also the separate contributions of the gravity and friction terms, as indicated by the detailed measurements performed. The distinction between these two terms becomes important in a transient approach of the problem, where they play quite different roles. The present steady-state model has been taken as a basis for a transient model developed for stability analysis, that will be presented in a later article.

Acknowledgements—This work was done under the auspices of the Direction des Réacteurs Nucléaires (Directorate of Nuclear Reactors) in the Département de Thermohydraulique et de Physique (Department of Thermalhydraulics and Physics).

REFERENCES

- Barnea, D. 1990 Effect of bubble shape on pressure drop calculations in vertical slug flow. *Int. J. Multiphase Flow* **16**, 79–89.
- Barnea D., Shoham, O., Taitel, Y. & Dukler, A. E. 1985 Gas-liquid flow in inclined tubes: flow pattern transitions for upward flow. *Chem. Eng. Sci.* **40**, 131–136.
- Belkin, H. H., Macleod, A. A. Monrad, C. C. & Rothfus, R. R. 1959 Turbulent liquid flow down vertical walls. *AIChE J.* **5**, 245–248.
- Brauner, N. & Barnea, D. 1986 Slug/churn transition in upward gas-liquid flow. *Chem. Eng. Sci.* **41**, 159–163.
- de Cachard, F. & Masbernat, F. 1987 Etude du fonctionnement, des air-lifts: étude bibliographique, expériences préliminaires et équations du régime permanent, Note Technique CEA/SETh/LEF 87-2.
- de Cachard, F. 1988 A developing slug flow model for small-diameter airlift pumps. *Proc. ANIMP Multiphase Flow Engineering Division Meeting, Bologna*, pp. 41–55.
- de Cachard, F. 1989 Etude théorique et expérimentale des instabilités des systèmes de pompage par air-lift, Thèse de Doctorat, INP Grenoble.
- Clark, N. N. & Dabolt, R. J. 1986 A general design equation for air lift pumps operating in slug flow. *AIChE J.* **32**, 56–64.
- Fernandes, R. C., Semiat, R. & Dukler, A. E. 1983 Hydrodynamic model for gas-liquid slug flow in vertical tubes. *AIChE J.* **29**, 981–989.
- Govan, A. H., Hewitt, G. F., Richter, H. J. & Scott, A. 1991 Flooding and churn flow in vertical pipes. *Int. J. Multiphase Flow* **17**, 27–44.
- Hewitt, C. F. & Hall-Taylor, N. S. 1970 *Annular Two-phase Flow*. Pergamon Press, Oxford.
- Idel'Chik, I. E. 1960 Handbook of hydraulic resistance, reproduced by National Technical Information Service, U.S. Department of Commerce.
- Jayanti, S. & Hewitt, G. F. 1992 Prediction of the slug-to-churn flow transition in vertical two-phase flow. *Int. J. Multiphase Flow* **18**, 847–860.
- Kouremenos, D. A. & Staïcos, J. 1985 Performance of a small air-lift pump. *Int. J. Heat Fluid Flow* **6**, 217–222.
- Lockhart, R. W. & Martinelli, R. C. 1949 Proposed correlation of data for isothermal two-phase, two-component flow in pipes. *Chem. Eng. Prog.* **45**, 39.
- Nakoryakov, V. E., Kashinsky, O. N. & Kozmenko, B. K. 1986 Experimental study of gas-liquid slug flow in a small-diameter vertical pipe. *Int. J. Multiphase Flow* **12**, 337–355.
- Nicklin, D. J., Wilkes, J. O. & Davidson, J. F. 1962 Two-phase flow in vertical tubes. *Trans. Inst. Chem. Engrs* **40**, 61–68.
- Reinemann, D. J., Parlange, J. Y. & Timmons, M. B. 1990 Theory of small-diameter airlift pumps. *Int. J. Multiphase Flow* **16**, 113–122.
- Ros, N. C. J. 1961 Simultaneous flow of gas and liquid as encountered in well tubing. *J. Pet. Techn.* **13**, 1037–1049.
- Taitel, Y., Barnea, D. & Dukler, A. E. 1980 Modelling flow pattern transitions for steady upward gas-liquid flow in vertical tubes. *AIChE J.* **26**, 345–354.

- Todoroki, I., Sato, Y. & Honda, T. 1973 Performance of air-lift pump. *Bull. JSME* **16**, 733–741.
- Wallis, G. B. 1969 *One Dimensional Two-phase Flow*. McGraw-Hill, New York.
- White, E. T. & Beardmore, R. H. 1962 The velocity of rise of single cylindrical air bubbles through liquids contained in vertical tubes. *Chem. Eng. Sci.* **17**, 351–361.
- Zuber, N. & Findlay, J. A. 1965 Average volumetric concentration in two-phase flow systems. *J. Heat Transfer* **87**, 453–468.